



HAL
open science

Eco-Friendly Synthesis of Nitrogen-Doped Mesoporous Carbon for Supercapacitor Application

Georges Moussa, Samar Hajjar-Garreau, Pierre-Louis Taberna, Patrice Simon,
Camelia Matei Ghimbeu

► **To cite this version:**

Georges Moussa, Samar Hajjar-Garreau, Pierre-Louis Taberna, Patrice Simon, Camelia Matei Ghimbeu. Eco-Friendly Synthesis of Nitrogen-Doped Mesoporous Carbon for Supercapacitor Application. Journal of Carbon Research, 2018, 4 (2), pp.20. 10.3390/c4020020 . hal-02465005

HAL Id: hal-02465005

<https://hal.science/hal-02465005v1>


Submitted on 14 Feb 2020

HAL is a multi-disciplinary open access archive for the deposit and dissemination of scientific research documents, whether they are published or not. The documents may come from teaching and research institutions in France or abroad, or from public or private research centers.

L'archive ouverte pluridisciplinaire **HAL**, est destinée au dépôt et à la diffusion de documents scientifiques de niveau recherche, publiés ou non, émanant des établissements d'enseignement et de recherche français ou étrangers, des laboratoires publics ou privés.

Article

Eco-Friendly Synthesis of Nitrogen-Doped Mesoporous Carbon for Supercapacitor Application

Georges Moussa^{1,2,3,4}, Samar Hajjar-Garreau^{1,2}, Pierre-Louis Taberna^{3,4}, Patrice Simon^{3,4}
and Camélia Matei Ghimbeu^{1,2,4,*} 

¹ Université de Haute-Alsace, Institut de Science des Matériaux de Mulhouse (IS2M) CNRS UMR 7361, F-68100 Mulhouse, France; georgesbmoussa@gmail.com (G.M.); samar.hajjar@uha.fr (S.H.-G.)

² Université de Strasbourg, F-67081 Strasbourg, France

³ Centre Interuniversitaire de Recherche et d'Ingénierie des Matériaux (CIRIMAT), UMR CNRS 5085, Université Paul Sabatier, 118 Route de Narbonne, F-31062 Toulouse, France; taberna@chimie.ups-tlse.fr (P.-L.T.); simon@chimie.ups-tlse.fr (P.S.)

⁴ Réseau sur le Stockage Electrochimique de l'Energie (RS2E), CNRS FR3459, 33 Rue Saint Leu, F-80039 Amiens CEDEX, France

* Correspondence: camelia.ghimbeu@uha.fr; Tel.: +33-389-608-743

Received: 16 February 2018; Accepted: 26 March 2018; Published: 30 March 2018



Abstract: A sustainable and simple synthesis procedure involving the co-assembly of green phenolic resin and amphiphilic polymer template in water/ethanol mixture at room temperature to synthesize nitrogen doped mesoporous carbon is reported herein. Guanine is proposed as a novel nitrogen-based precursor which is able to create H-bondings both with the phenolic resin and the template allowing the formation of mesoporous carbons with nitrogen atoms uniformly distributed in their framework. The influence of the synthesis procedure, template amount and annealing temperature on the carbon textural properties, structure and surface chemistry were investigated. For several conditions, carbon materials with ordered pore size and high nitrogen content (up to 10.6 at %) could be achieved. The phase separation procedure combined with optimal amount of template favor the formation of ordered mesoporous carbons with higher specific surface area while the increase in the temperature induces a decrease in the surface area and amount of heteroatoms (N and O). The electrochemical performances as electrode in supercapacitors were evaluated in acidic medium and the capacitance was closely related to the material conductivity and surface chemistry.

Keywords: N-doped mesoporous carbon; soft-template; guanine; supercapacitor

1. Introduction

Ordered mesoporous carbons (OMC) received tremendous attention during the last decade mainly due to their tunable and uniform pore size/geometry, pore connectivity and adjustable surface functionalities. All these properties made them valuable materials in many fields of applications such as the catalysis, gas adsorption and separation, energy storage, drug delivery, and gas sensors [1–7]. The design of ordered carbon materials can be achieved only via two specific synthesis pathways, i.e., the hard and soft-template. Herein, the soft template has been chosen taking into consideration the advantages such as simplicity, time efficiency and convenient removal of the template by simple thermal annealing. This approach consists in supramolecular self-assembly organization of organic species. In general, cross-linked phenolic resins are used as carbon-yielding components, which are able to co-assembly with an amphiphilic block co-polymer acting as a pore-forming component. Thermopolymerization of such assemblies allows the formation of a thermosetting phenolic resin and further thermal annealing induces the decomposition of the phenolic resin and of the soft template

resulting in a mesoporous carbon formation. Due to the flexibility of this synthesis, the incorporation of other species is very simple allowing to obtain heteroatom's doped or hybrid mesoporous carbons.

In the recent years, nitrogen became the most studied heteroatom since it allows to enhance carbon electronic conductivity, surface polarity and electron-donor tendency, improving the carbon performances in different applications. N-doped porous carbons show great potential in energy storage and they are particularly used in supercapacitors [8] which are known to be environmentally friendly and a high safety system combining high power density [9] and long cycling life [10]. Depending on the charge storage mechanism, two types of supercapacitors are known [11], i.e., electrical double layer capacitors (EDLC) where the charge is stored at the carbon/electrolyte interface and redox-based electrochemical capacitors [12–15] where the charge is stored via redox reactions promoted by the material in the presence of the electrolyte. While in the first case, the performances are related to the carbon porosity [16–18], in the second case they are affected by the carbon surface chemistry [19], namely, the nature and amount of functional groups. Therefore, it appears that the combination of an optimal carbon porosity and surface chemistry must be achieved in order to improve the electrochemical performances [12,15,16,20].

N-doped mesoporous carbons can be synthesized by post-synthesis routes involving the impregnation of a carbon with urea, melamine or polypyrrole, followed by thermal annealing under inert atmosphere or by direct exposure to ammonia gas at high temperatures [8]. However, these methods are generally time consuming and costly for practical application and for this reason the direct thermal transformation of nitrogen containing polymers into N-doped carbon was also explored. Wei et al. [21] reported the synthesis of N-doped mesoporous carbon using the evaporation-induced self-assembly (EISA) process and phenol-formaldehyde derived resol as carbon source, Pluronic F-127 as template and dicyandiamide as nitrogen source. The carbon resol and dicyandiamide were able to assemble with the micelles of pluronic template via hydrogen bonding and electrostatic interactions giving rise after thermal annealing to N-doped mesoporous carbon presenting tunable mesostructures, pore size and high nitrogen content (13.1 wt %). Wang et al. [22] proposed the use of aminophenol as carbon and nitrogen source, formaldehyde as cross-linker and pluronic F-127 as pore agent. The co-assembly of these molecules resulted in N-doped mesoporous carbon with a hexagonal structure and nitrogen amount of 3.3 at %. By employing aminophenol, hexamethylenetetramine (HMTA), formaldehyde and Pluronic F-127, Chen et al. [23] demonstrated successful synthesis of single crystals of N-doped mesoporous carbon through a soft-template approach. Yu et al. [24] used urea as nitrogen source, hexamethylenetetramine, resorcinol-formaldehyde and pluronic F-127 co-assembled in an aqueous ammonia solution in a soft-template route under hydrothermal conditions. N-doped mesoporous carbon exhibiting a cubic structure and ~2.5 wt % of nitrogen was obtained. Using the same soft-template approach assisted by hydrothermal conditions, nitrogen-doped carbon could be obtained by self-assembly of poly(benzoxazine) with resorcinol-formaldehyde resin and lysine as precursors [25,26]. Melamine-formaldehyde resins [27,28] and aniline [29] were reported as well as nitrogen source for the preparation of N-doped mesoporous carbons.

The main inconvenience presented by the above mentioned synthesis pathways are related either to the use of toxic precursors (phenol, formaldehyde, aniline ...), or strong acids/bases for the polymerization of phenolic resin and hydrothermal conditions for rigidifying the resin. Therefore, developing more environmentally friendly synthesis routes involving limited synthesis steps and that can be cost-effective for large-scale applications are of great need. In this aim, significant progress was made by our group in the recent years to improve the soft-template route. Firstly, the glyoxylic acid as a green precursor extracted from plants was proposed for the first time as cross-linker alternative instead of formaldehyde with no requirements of supplementary base/acid catalyst in the synthesis. Such a green synthesis pathway was successfully used to prepare mesoporous carbon powders and films with tuned pore size and geometries, various graphitization levels via classical approaches like EISA and phase separation [30], but also by novel more unconventional routes assisted by light [31,32]. Recently two green approaches have been developed to prepare N-doped porous carbon.

Phloroglucinol/glyoxylic acid resin was cross-linked with triethylenediamine (TEDA) as nitrogen source in water at room temperature and in the absence of a template, resulting in the formation of microporous carbon spheres [33]. Chitosan, a biocompatible and green precursor was as well proposed as a simultaneous carbon and nitrogen precursor which was able to assemble with Pluronic F-127 template to obtain N-doped carbon beads with hierarchical porosity by a soft-template assisted by a freezing-drying technique [34].

Inspired by our recent works, herein, we report a direct synthesis of N-doped ordered mesoporous carbons with a high nitrogen content and tuned porosity by co-assembly of phloroglucinol–glyoxylic acid resin and guanine with Pluronic F-127 template in water/ethanol mixture at room temperature. Guanine is proposed as a new green precursor which contains high nitrogen content (46.3%) coming from one nitrile group and two amine groups in its composition. Several synthesis parameters were investigated (synthesis procedure, template amount and annealing temperature) and their impact on the final material texture and structure finely characterized. Thus, insight on the formation mechanism of the N-doped mesoporous carbon using guanine is proposed based on several techniques. Selected materials were tested as supercapacitors and the performances are discussed in terms of materials characteristics.

2. Materials and Methods

2.1. Material Synthesis

All chemicals were purchased from Sigma-Aldrich (Darmstadt, Germany) and used as received without any further purification. The nitrogen doped carbon porous materials were synthesized by soft-templating approach. Typically, phloroglucinol (0.82 g) and Pluronic F-127 (1.6 g) were dissolved in an ethanol/water mixture (15/30 mL) followed by the addition of guanine (0.46 g) and glyoxylic acid (0.53 g). Three different procedures were investigated: (i) a phase separation approach consisting in aging the mixture in the absence of stirring during 48 h at normal conditions of pressure and temperature; (ii) a stirring approach, a rather similar procedure as before but in this case the solution is stirred continuously in a closed Teflon beaker; and (iii) a stirring/evaporation approach implying the evaporation of the solvent under stirring in air in a fume-hood using the same Teflon beaker but uncovered. The obtained polymer-gel was recovered (in the first two cases the solvent must be discarded) and dried at room temperature and at 80 °C in air for 12 h followed by another 12 h at 150 °C in order to cross-link the phenolic resin framework. The obtained materials were pyrolyzed at 600 °C under inert atmosphere (Ar) for 1 h using a heating rate of 2 K/min. To check the influence of annealing temperature, two other temperatures were investigated, i.e., 750 and 900 °C on the materials obtained using the stirring method. Another studied parameter was the amount of Pluronic F-127 template, i.e., 0.8 and 0.4 g was used in addition to the reference quantity 1.6 g. A last material was prepared in the absence of phloroglucinol in order to evaluate the contribution of guanine in the synthesis mechanism. The amounts of guanine and glyoxylic acid was increased to 0.8 g while that of template, Pluronic F-127 was kept constant (1.6 g).

2.2. Material Characterization

The textural properties of the carbon material were investigated with Micromeritics ASAP 2420 Accelerated Surface Area and Porosimetry System (Micromeritics Instrument Corporation, Norcross, GA, USA) using N₂ as adsorbate at −196 °C and allowing simultaneous analysis of six materials. Prior to the analysis, the samples were out-gassed overnight under vacuum at 300 °C on the degassing port followed by 12 h out-gassing on the analysis port. The specific surface area (SSA) was calculated from the linear plot in the relative pressure range of 0.05–0.3 using the BET (Brunauer–Emmett–Teller) model while the micropore volume (V_{micro}) was determined using the Dubinin–Radushkevich (DR) equation. The mesopore volume (V_{meso}) was obtained by subtracting the micropore volume from the total pore volume of N₂ adsorbed at a relative pressure P/P_0 of 0.95. The pore size distributions (PSD)

were determined from the adsorption branch of nitrogen isotherms using the 2D-NLDFT (non local density functional theory) standard slit pore model for carbon materials implemented in SAIEUS software (Micromeritics) [35,36].

The long-range ordering of the materials was studied by small angle X-ray scattering (SAXS) analysis using a Rigaku SMax 3000 (RIGAKU, Tokyo, Japan) equipped with a rotating Cu anode Micromax-007HF (40 kV, 30 mA) and OSMIC CMF (Confocal Max Flux) optics. ImageJ software (National Institutes of Health, Rockville Pike, MD, USA) was used for SAXS treatment of different images collected with the X-ray 2D detector. X-ray photoelectron spectroscopy (XPS) was performed with a VG Scienta SES 200-2 spectrometer (VG Scienta, Uppsala, Sweden) equipped with a monochromatized Al K α X-ray source (1486.6 eV) and a hemispherical analyzer (VG Scienta, Uppsala, Sweden). Widescan and high resolution XPS spectra are recorded with a pass energy 100 eV. Spectra were subjected to a Shirley baseline and peak fitting was made with mixed Gaussian-Lorentzian components with equal full-width-at-half-maximum (FWHM) using CASAXPS version 2.3.17 software (Neal Fairley, Teignmouth, UK). All the binding energies (BE) are referenced to the C1s peak (sp² carbon atoms) from the "graphitic material" at 284.6 eV.

The material surface morphology/structure was investigated with a JEOL ARM-200F transmission electron microscope (TEM) (JEOL, Akishima, Japan) working at 200 kV. Energy Dispersive X-ray analysis (EDX) mapping with quantitative determination of atomic composition of the NPs was obtained with a JED 2300 detector (JEOL, Akishima, Japan) coupled with the transmission electron microscope.

¹³C solid-state NMR CP-MAS (cross-polarization magic angle spinning) experiments have been performed on a Bruker Avance 400 MHz spectrometer (Bruker, Karlsruhe, Germany) using 3.2 mm zirconia rotors spinning at a MAS frequency of 13 kHz. Recycle delay for all CP experiments was 4 s and spinal-64 decoupling was applied during signal acquisition. Cross-polarization transfers were performed using adiabatic tangential ramps to enhance the transfer efficiency, and the contact time was 1 ms.

2.3. Material Electrochemical Characterization

The materials were tested using Swagelok cells in a 2-electrode configuration, by cyclic voltammetry using a multichannel VMP3 potentiostat/galvanostat (Biologic, Paris, France). Electrodes were prepared by mixing 95% of carbon with 5% of polytetrafluoroethylene (PTFE) binder in the presence of ethanol. In some cases, carbon black was used (30 wt %). Electrochemical capacitors were built using two carbon electrodes (8 mm diameter) with comparable mass (~7 mg) and thickness (200 μ m) [37] which were electrically isolated by a 50 mm-thick porous cellulose as separator disk. As counter electrode a platinum disk was used. All materials were tested in 0.1 M H₂SO₄ aqueous electrolyte. Cyclic voltammetry was performed in a voltage window between 0 and 0.9 V for aqueous electrolytes at scan rates of 20 mV·s⁻¹. Electrochemical impedance spectroscopy (EIS) measurements were carried out at open-circuit voltage within the frequency range from 1 mHz to 100 kHz.

3. Results and Discussion

The synthesis of N-doped carbons was performed via the soft-template approach involving the organic-organic self-assembly of phenolic resins molecules with a soft-template (triblock polymer, Pluronic F-127), which is able to create the mesoporosity and to organize it in different shapes and size depending of several factors (Figure 1).

Herein, few important parameters have been explored in order to evaluate their influence on the final carbon characteristics. The phase separation, even if less used compared to the EISA method, was selected for this study taking into consideration the following advantages (a) allows to prepare high quantities of material per batch of synthesis, therefore possible to up-scale and (b) easy to perform and to recover the polymer for carbonization (scratching of polymer film from petri dishes being necessary for EISA method). However, the control of porosity (surface area, pore size and architecture)

is of great importance, particularly when new precursors are incorporated in the synthesis mixture. This is the case of guanine which was used for the first time in order to introduce nitrogen in the carbon framework.

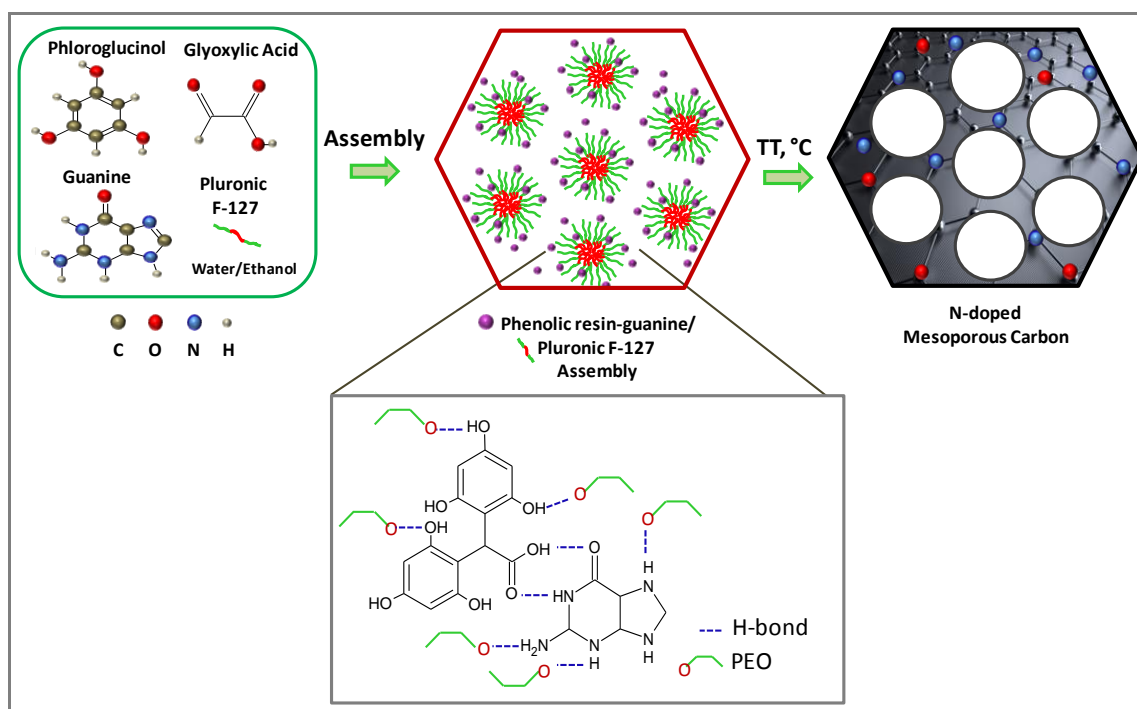


Figure 1. Schematic representation of the synthesis process of N-doped mesoporous carbon and the involved mechanism.

Firstly, the impact of the synthesis type on the carbon porosity was investigated and three different procedures were evaluated: (a) the phase separation, involving macroscopic phase separation of polymeric resin and the solvent; (b) phase separation assisted by stirring, herein “stirring”; and (c) stirring/evaporation method, a similar approach as method (b) but being conducted in an uncovered vessel to allow complete evaporation of the solvent. The as-obtained gels after the synthesis were thermopolymerized and pyrolyzed and the obtained carbons analyzed by transmission electron microscopy (Figure 2). The carbon obtained by phase separation (Figure 2a) present regular parallel channels indicating an ordered porous structure. When the synthesis is assisted by stirring (Figure 2b), the morphology became less ordered or even completely disordered when the synthesis is performed under evaporation (Figure 2c). This result indicates that the way of synthesis preparation has a great impact on the mesoporosity formation.

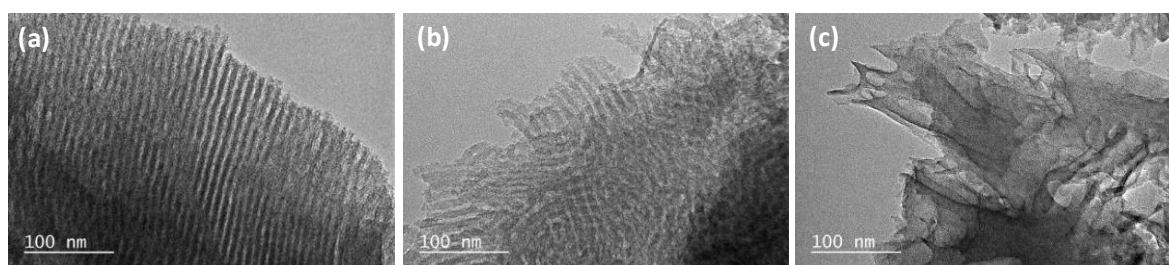


Figure 2. TEM images of carbon materials obtained by using different synthesis procedures: phase separation (a), stirring (b) and stirring/evaporation (c).

To obtain further details about the materials porosity, nitrogen adsorption measurements were performed and the obtained nitrogen adsorption/desorption isotherms are shown in Figure 3a. For the materials prepared by phase separation and stirring, the isotherms present a type IV shape with a hysteresis loop of type 2 between 0.4 and 1, P/P_0 relative pressure, confirming the mesoporous character of the materials. An increase of the adsorbed nitrogen volume in the low relative pressure region is observed as well suggesting the presence of micropores. Comparing the two materials, it can be noticed that the microporous part is rather similar, slightly higher in the case of carbon obtained by stirring which translates in the same tendency for specific surface areas (445 and 570 $\text{m}^2 \cdot \text{g}^{-1}$ for phase separation and stirring, respectively) and microporous volume (0.19 vs. 0.25 $\text{cm}^3 \cdot \text{g}^{-1}$, Table 1). If the mesoporous part of the isotherms are compared ($P/P_0 > 0.4$), it can be clearly seen a much defined hysteresis with higher adsorbed nitrogen volumes for phase separation derived carbon. This implies that this carbon presents a more developed mesoporosity as confirmed by the determination of mesoporous volume which is 0.50 $\text{cm}^3 \cdot \text{g}^{-1}$, therefore five times higher than in the case of stirring derived carbon, 0.11 $\text{cm}^3 \cdot \text{g}^{-1}$. The mesopore size is different as well (Figure 3b), ~ 4 nm and 8 nm for phase separation and stirring, respectively. The micropores are visible on the pore size distribution, with sizes less than 1 nm for both materials. As the mesoporosity is much affected by the stirring procedure compared to microporosity, we can believe that this had an effect on the self-assembly of the phenolic resin with the template rather than on the formation of the resin. As a reminder, the thermal decomposition of phenolic resin (cross-linked phloroglucinol with glyoxylic acid) is responsible for the micropore creation while the decomposition of the template is related to the mesoporous formation [38]. Surprisingly, if the stirring synthesis is assisted by evaporation, the resulting carbon material is not porous, the surface being very small (36 $\text{m}^2 \cdot \text{g}^{-1}$). Therefore, the cross-linking of the phloroglucinol with glyoxylic acid and the self-assembly of the resulting resin with the template is strongly affected by the evaporation of the solvent. Taking into consideration the higher evaporation rate of ethanol over water, we can expect that the removal of ethanol is done before the water and that the polymer solution will be enriched in water solvent. As some precursors, such as phloroglucinol have limited solubility in water, it can be supposed that its cross-linking with glyoxylic acid and further self-assembly with the template is not promoted. However, at this point the mechanism behind the porosity loss is not yet clear, but it is evident that this approach is detrimental for the preparation of carbons with controlled porosity. Therefore, we select the stirring procedure to investigate further the template amount influence.

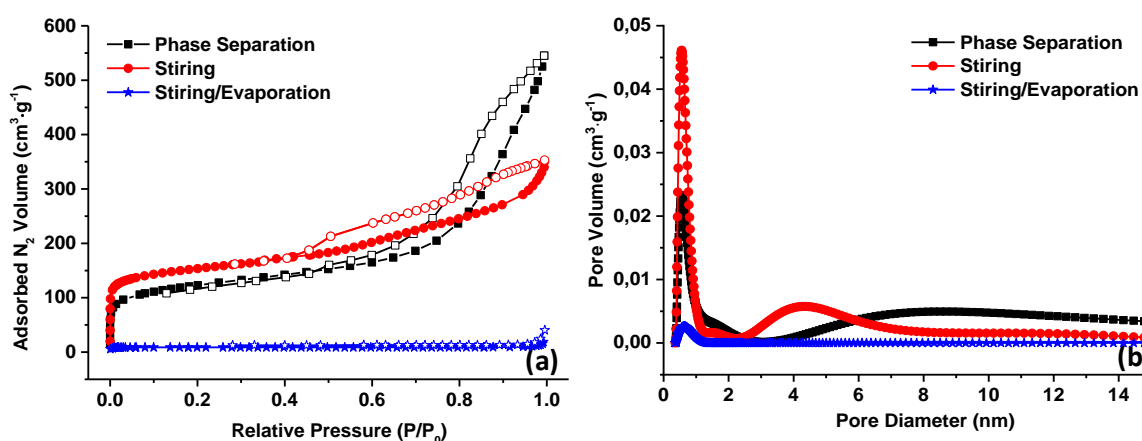


Figure 3. Nitrogen adsorption/desorption isotherms (a) and their corresponding 2D-NLDFT pore size distribution (b) of carbon materials obtained by using different synthesis procedures.

Table 1. Textural properties of carbon materials determined from N₂ adsorption/desorption isotherms.

Materials	SSA m ² ·g ⁻¹	Vt cm ³ ·g ⁻¹	V _{micro} cm ³ ·g ⁻¹	V _{meso} cm ³ ·g ⁻¹
Phase Separation	445	0.69	0.19	0.50
Stirring	570	0.46	0.25	0.11
Stirring/Evaporation	36	0.016	-	-
1.6	570	0.46	0.25	0.11
0.8	523	0.67	0.22	0.40
0.4	341	0.42	0.13	0.29
600	523	0.67	0.22	0.40
750	587	0.63	0.22	0.41
900	322	0.35	0.12	0.23

Figure 4 presents the TEM images and the small-angle X-ray scattering of carbon materials resulting by changing the initial amount of template from 1.6 g to 0.8 g and 0.4 g, respectively. It can be observed in the TEM pictures that diminishing the quantity from 1.6 g (Figure 4a, left) to 0.8 g (Figure 4b, left), the morphology changes, an ordered material presenting uniform parallel channels with ordered distributed porosity (in-set) being obtained. However, if the quantity is further decreased to 0.4 g, the obtained material is more disorganized (Figure 4c, left) compared the other two materials. These results are sustained by the SAXS measurements, showing a well-defined diffraction peak at around 0.8° 2theta for 0.8 g materials. This peak corresponds to the 10 diffraction planes of a 2D hexagonal ordered mesostructure having *p6m* symmetry [30]. On the contrary, only a small peak is seen for 1.6 g material and no peak for 0.4 g material indicating low ordering in line with the TEM observations.

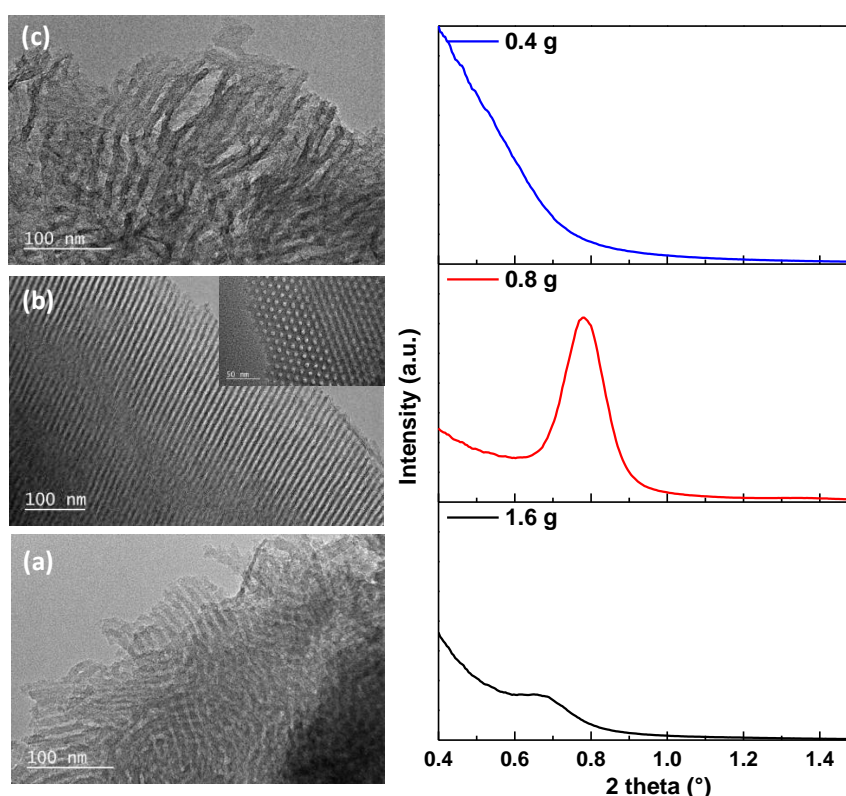


Figure 4. (left) TEM images of carbon materials and (right) Small-angle X-ray Scattering patterns of carbon materials obtained using the stirring procedure and different amounts of template: 1.6 g (a), 0.8 g (b) and 0.4 g (c).

The nitrogen adsorption/desorption isotherms show for all materials type IV isotherms specific to micro/mesoporous materials (Figure 5a). For 1.6 and 0.8 g, the low-pressure curves are almost overlapped, inducing similar microporosity (V_{micro} , Table 1) and SSA (570 vs. 527 $\text{m}^2\cdot\text{g}^{-1}$, respectively), while the high pressure region corresponding to the mesopores is much developed for 0.8 g material (0.11 vs. 0.40 $\text{cm}^3\cdot\text{g}^{-1}$ for 1.6 and 0.8 g material, respectively). For 0.4 g material, the mesoporosity is similar with 1.6 g material while the microporosity and the SSA is the smallest one among the studied materials (341 $\text{m}^2\cdot\text{g}^{-1}$, Table 1). The pore size is also different depending on the template amount as demonstrated in Figure 5b. This suggests that a certain quantity of template is required to obtain high surface area materials with ordered porosity. This is a balance between the formations of ordered template micelles able to interact with the phenolic resin through H-bondings. The 0.8 g material is therefore the most interesting one to investigate further the impact of annealing temperature on the porosity but also on the surface chemistry.

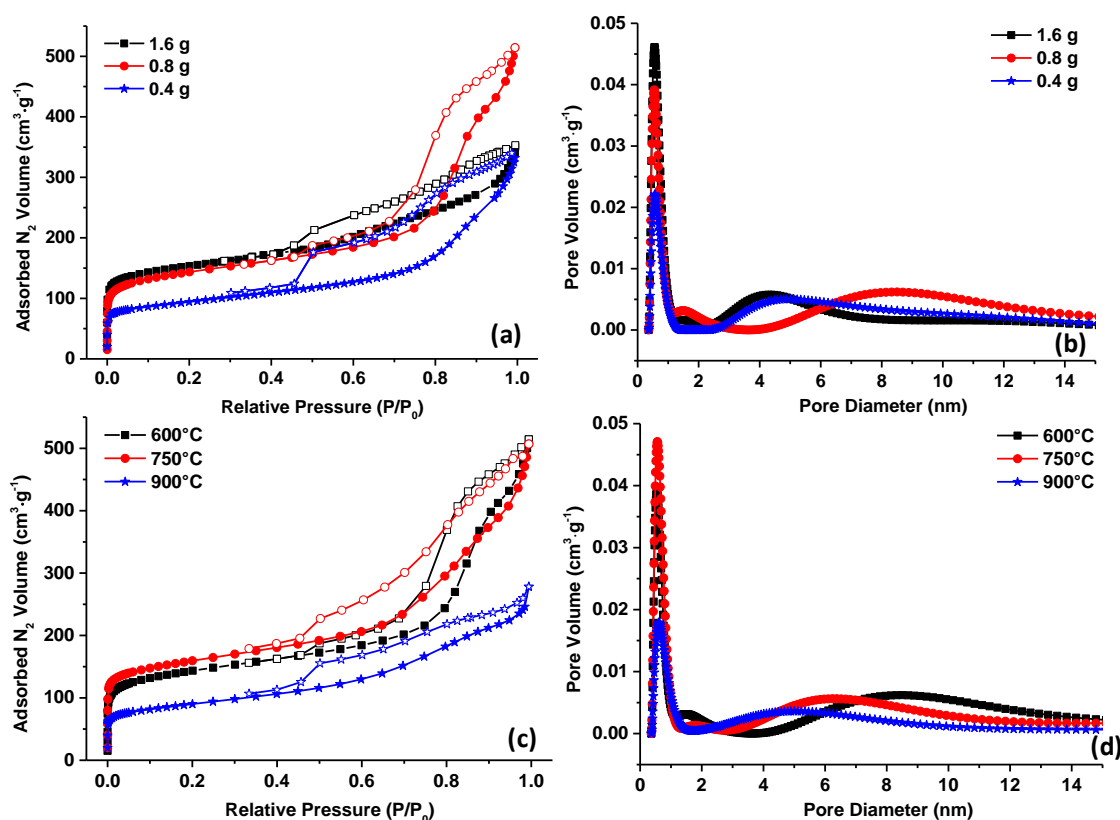


Figure 5. Nitrogen adsorption/desorption isotherms and the corresponding 2D-NLDFT pore size distribution of carbon materials obtained by using the stirring procedure and different amounts of template (a,b) and different temperatures (template amount 0.8 g) (c,d).

The nitrogen adsorption/desorption measurements for carbon materials were prepared at standard 600 °C but also at higher temperatures 750 °C and 900 °C, depicted in Figure 5c. For 600 and 750 °C, the shapes of the curves are similar, slightly higher for 750 °C resulting in similar textural values as seen in Table 1. Increasing the temperature to 900 °C has a negative impact on the porosity, the SSA being reduced from 587 (750 °C) to 322 $\text{m}^2\cdot\text{g}^{-1}$ (900 °C). The pore size is affected as well by the temperature as shown in Figure 5d. The micropore size is increasing from 0.54 nm for 600 °C to 0.62 nm for 900 °C, while for the mesopores an opposite behavior is seen, i.e., shrinkage from ~9 nm to 7 nm and 5 nm for 600, 750 and 900 °C materials, respectively. The modification of pore size can be in some extent related to the collapse of the micropores with the formation of larger one and to the densification of the carbon matrix due to the removal of heteroatoms. This last aspect was analyzed

in more detail since it may also influence the electrochemical performances of the supercapacitors. The heteroatoms may change the wettability behavior of the material with the electrolyte, the electronic conductivity and may induce redox reactions with the electrolyte.

In this aim, the XPS analyses were performed for the carbon treated at different temperatures. The survey spectra were recorded and besides the carbon presence, oxygen and nitrogen were detected. For 600 °C material, the C, O and N contents are 83.4, 6.2 and 10.4 at % respectively. It is worth noting, the high quantity of nitrogen that could be introduced by using the guanine. Increasing the temperature to 900 °C, both the oxygen and nitrogen amount are reduced to ~4 and 6 at %, respectively (Table 2). The high-resolution spectra of C1s were deconvoluted in several components (Figure 6, left). The most intense one is related to Csp² followed by C=N and C–N bonds [39,40]. The increase of the full width at half maximum (FWHM) of the C1s peak at 600 °C compared to 700 °C and 900 °C, and the appearance of a peak towards 286.5 eV, is related to the presence of oxygen functional groups such as ethers, carbonyl, carboxyl (–C–OR, –C=O and O=C–O) and nitrogen groups (C=N, C–N), which are located at higher binding energy compared to the Csp².

Table 2. Carbon composition as determined by XPS analysis and electrochemical capacitance extracted from cycling voltammetry curves.

Materials	C, at %	O, at %	N, at %	Capacitance, F·g ^{−1}	ESR, ohm
600 °C	83.4	6.2	10.4	0.6	8150
750 °C	90.1	3.1	6.7	84	13
900 °C	89.3	4.5	6.1	53	6.0
750 °C-CB	-	-	-	95	4.0

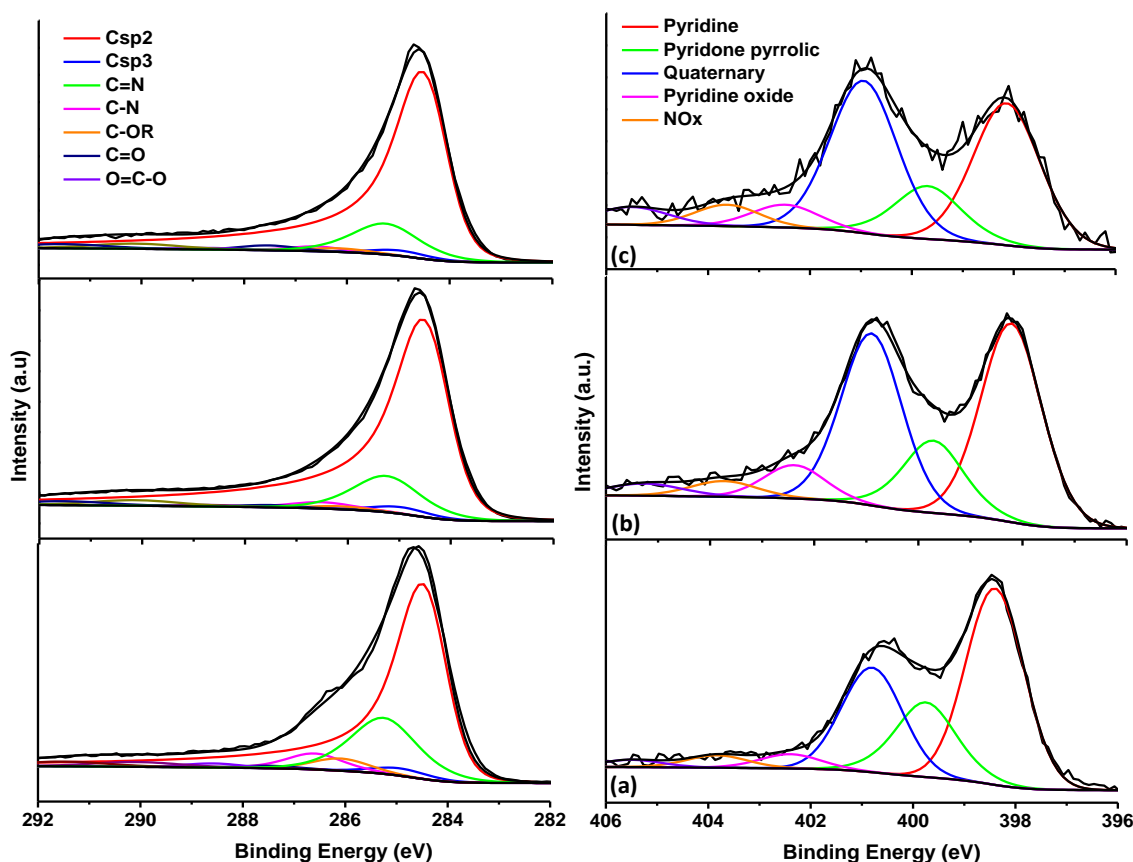


Figure 6. XPS deconvoluted spectra of the stirring procedure and different annealing temperatures (a) 600 °C, (b) 750 °C and (c) 900 °C.

Increasing the temperature, the FWHM of C1s peak decreases due to the removal of some oxygen and nitrogen groups. In addition, the N1s peaks exhibit five contributions located at 398.1, 399.6, 400.9, 402.5 and 403.6 eV (Figure 6, right) corresponding to pyridine, pyridine pyrrolic, quaternary, pyridine oxide and NO_x nitrogen functional groups [40,41]. At 600 °C, the pyridine groups are predominant while increasing the temperature they are partly removed leaving place to quaternary groups which become predominant at 900 °C.

The distribution of N and O atoms in the carbon framework was evaluated by EDX mapping (Figure 7) and it can be observed that the heteroatoms are very well distributed in the carbon matrix at atomic level. This indicates a good repartition of the guanine in the phenolic resin resulting in a uniform N-doped carbon.

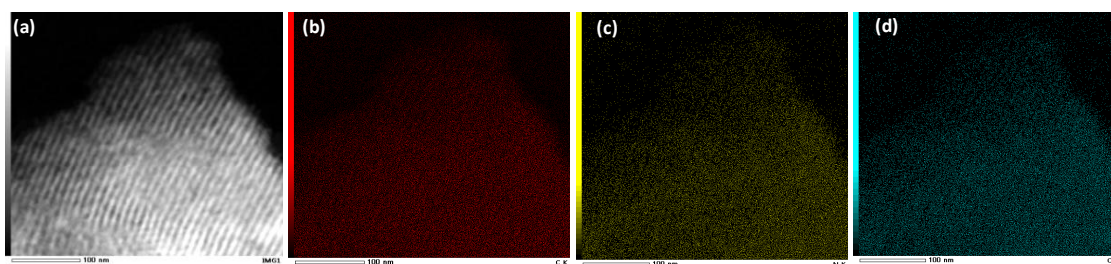


Figure 7. STEM image of a typical carbon (a) along with the EDX mapping showing the distribution of C (b), N (c) and O atoms (d) in the materials.

To get further insights on the formation of these materials, ¹³C NMR was performed on a phenolic resin containing guanine and in addition for comparison purposes on a phenolic resin which is free of guanine and on guanine precursor (Figure 8). The ¹³C NMR of guanine exhibit three main peaks placed at 156, 141 and 106 ppm, respectively. The first peak (156 ppm) is the most intense one and correspond to carbon atoms bonded to oxygen (=O) in the pyrimidine cycle. The peak presents a shoulder which assigned to saturated and unsaturated carbon atoms bonded to nitrogen pyrimidine cycle (in-set Figure 8).

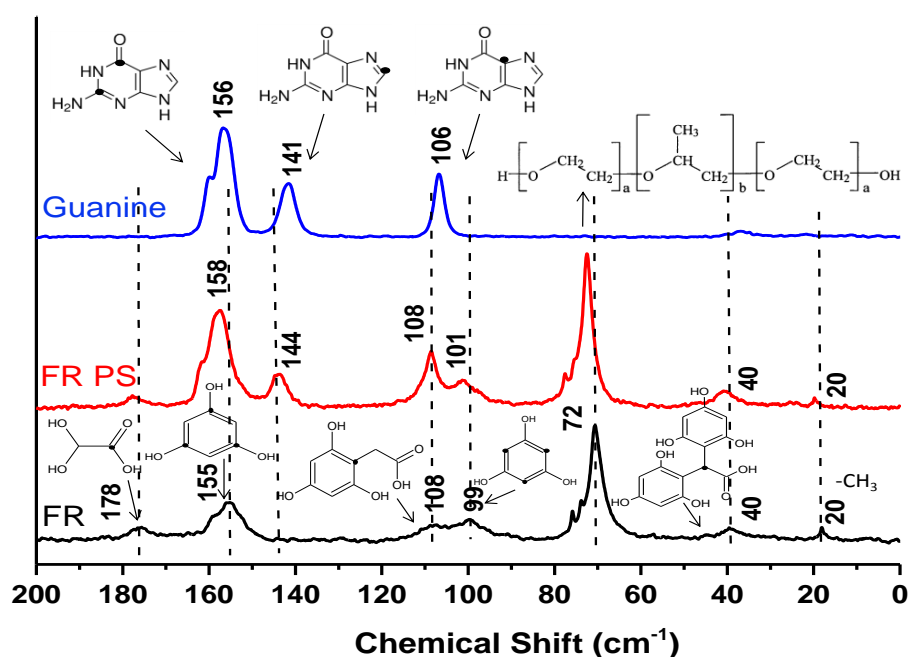


Figure 8. ¹³C CPMAS NMR spectra of (a) guanine, (b) phenolic resin PS containing guanine (FR PS) and (c) phenolic resin (FR) prepared without guanine.

The peak for 141 ppm is related to the carbon atoms bonded to nitrogen in the imodazole cycle, while the peak placed at 106 ppm is assigned to carbon atoms bonded simultaneous with carbonyl groups and nitrogen atoms. The NMR conducted on phenolic resin containing guanine (FR PS) confirms the presence of guanine by the appearance of the three peaks mentioned before. In addition, other peaks are seen at 178, 158 and 101 ppm, which are mainly related to the carbon atoms present in the initial precursors (phloroglucinol and glyoxylic acid) suggesting still some un-reacted precursors. Another two peaks are detected at 108 and 40 ppm indicating cross-linked phloroglucinol with glyoxylic acid via covalent bondings. The detailed mechanism of cross-linking was previously reported in our works [30,32,38]. An intense contribution is seen at ~72 ppm and a small one at 20 ppm corresponding to the carbons atoms in $-CH$, $-CH_2$ and $-CH_3$ groups present in the PPO (polypropylene oxide) and PEO (polyethylene oxide) moieties of the Pluronic F-127 template. It is worth noting that if we compare all three NMR spectra, the spectra of phenolic resin containing the guanine is an addition of the spectra of guanine and phenolic resin (FR). No supplementary peaks appear indicating no cross-linking reactions by covalent bonds between the guanine and the phenolic resin, as for instance may occur by using another nitrogen precursor as recently demonstrated [33]. As well, a simple physical mixture between the guanine and the phenolic resin can be excluded taking into consideration the TEM and EDX results showing the formation of ordered carbon materials with uniform distribution of nitrogen in their framework.

The most plausible hypothesis to explain the formation of these materials is the creation of H-bonding between the guanine and the phenolic resin and the template. This scenario is possible since the guanine is well known to be able to create H-bondings with various compounds. The carbonyl bond ($=O$) of guanine may act as a hydrogen bond acceptor and may create H bonds with the $-OH$ groups of phloroglucinol while the nitrogen groups ($-NH$ and $-NH_2$) may act as a hydrogen bond donor which may favor the H-bonding with the carbonyl groups ($=O$) of glyoxylic acid or its derivatives. The as-formed phenolic resin/guanine system may further assemble by H-bondings with the micelles of Pluronic template. Two main possibilities of assembly of phenolic resin/guanine system with the template are possible. On one hand the high number of hydroxyl groups ($-OH$) of phloroglucinol and on the other hand the $-NH$ and $-NH_2$ groups of guanine, may develop H-bonds with the $-O$ of PEO fragments of the template. In the water/ethanol solution, the PPO fragments of the template form the core of the micelles while the PEO the shell of the micelle. The phenolic resin/guanine may form H-bonding with the oxygen atoms coming from the hydrophilic PEO moieties of the pluronic micelle shell, forming a layer of resin/guanine in the surface of the micelles.

To evaluate if the guanine can self-assemble with the template we performed a supplementary synthesis where phloroglucinol was not used. Surprisingly, the resulting material is porous (Figure 9a) and this porosity is randomly organized than compared to the carbon obtained in the presence of phloroglucinol (Figure 9b). This demonstrates that guanine itself is able to create H-bonding and to assemble with the Pluronic template, and this assembly involves different bonds compared to phloroglucinol. In addition, guanine can be used both as nitrogen but also carbon source.

Taking into considerations these results, one can propose that the synthesis of N-doped mesoporous carbon proceed by a complex multi-component co-assembly process where the carbon precursors (the phenolic resin), the nitrogen source (guanine) and the pore agent (Pluronic F-127) are closely interacting by H-bondings. Further thermal annealing of such assembly, decompose the template and allow to obtain a mesoporous carbon with nitrogen in its structure. A general schema resuming the synthesis mechanism of assembly of phenolic resin/guanine and the template is proposed in Figure 1.

The electrochemical performances of several N-doped carbon materials synthesized at 600 °C were evaluated in a two-electrode configuration in 0.1 M H_2SO_4 electrolyte in the potential range of 0–0.9 V using a scan rate of 20 mV s^{-1} . Cycling voltammetry was used to study the electrochemical behavior and a typical curve for a material prepared at 600 °C is presented in Figure 10a. Surprisingly, the capacity value was found to be close to zero F/g, however, increasing the annealing temperature

to 750 and 900 °C, the cyclic voltammetry (CV) curve shape improves and the capacitance as well, i.e., 84 F/g and 53 F/g for 750 °C and 900 °C.

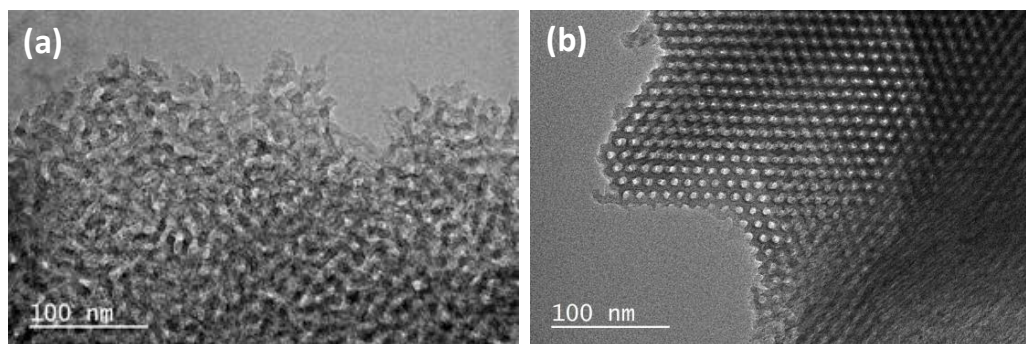


Figure 9. TEM images of carbon materials obtained in the absence (a) and presence (b) of phloroglucinol.

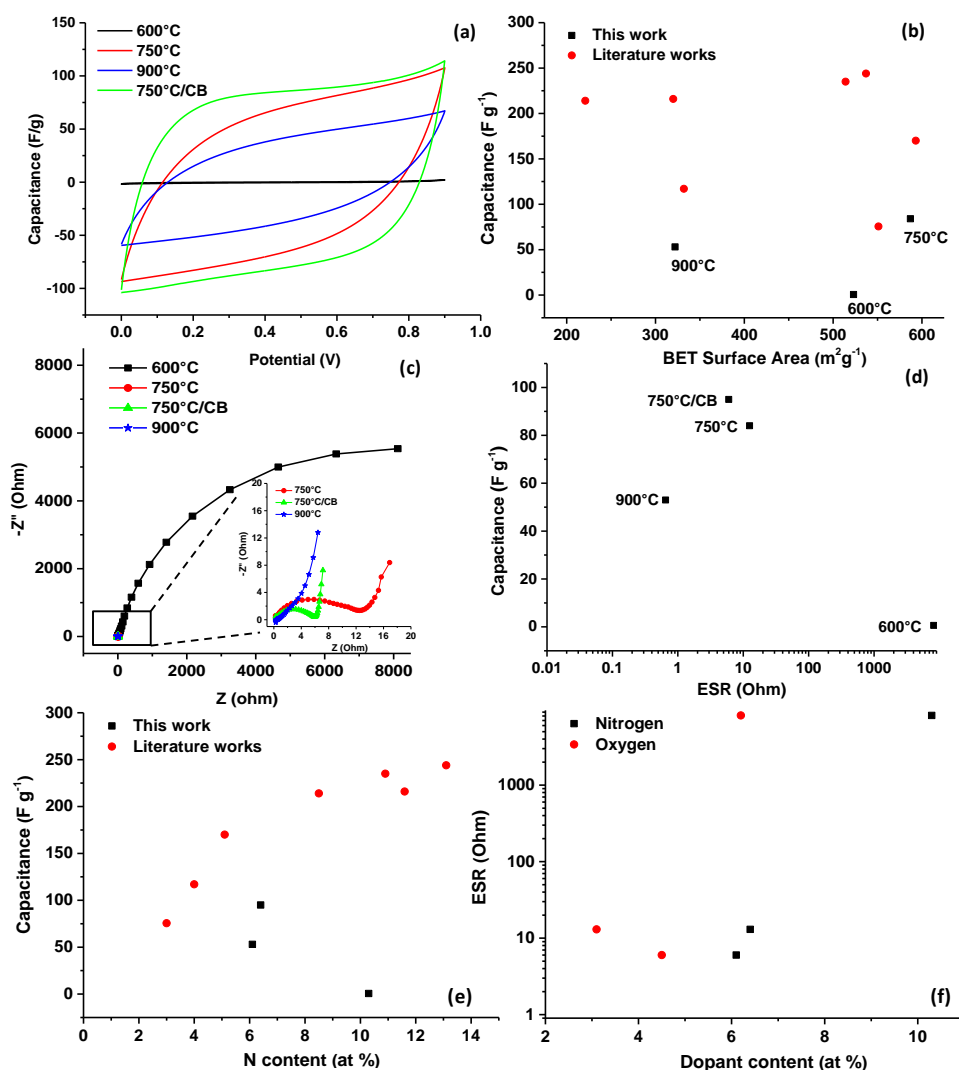


Figure 10. Electrochemical cyclic voltammetry (a) and electrochemical impedance spectroscopy, Nyquist plots (c) along with the evolution of capacitance vs. BET surface area (b) ESR (d) and nitrogen content (e) of nitrogen-doped carbons prepared in this work and from the literature; evolution of ESR vs. nitrogen and oxygen content in the materials (f).

To explain this behavior several important factors must be considered such as porosity and surface chemistry. Concerning the porosity, it has been seen before that this similarity between 600 °C and 750 °C, slightly higher for the latest one while for 900 °C, the porosity is significantly lower than at 600 and 750 °C (Figure 10b). Therefore, the textural properties cannot explain why the capacitance of 600 °C sample is very low. On the other hand, the XPS showed for the 600 °C a high amount of nitrogen and oxygen groups compared to 750 and 900 °C samples (Table 2). The high number of functional groups are supposed to have a positive effect on the wettability of carbon surface with the electrolyte as well in promoting redox reactions to improve the capacitance by pseudocapacitive effects. However, particularly the oxygen groups may be detrimental to the electronic conduction of the material. To get more insights on this aspect, EIS was performed and the Nyquist plots are shown in Figure 10c.

A large semicircle in the high to low frequency region is seen for 600 °C sample indicating a highly resistive material, which can be accounted to the large amount of oxygen. Increasing the temperature to 750 °C, the shape of the curve changes to a semicircle in the high-to-medium frequency range, accompanied by a sloped line in the low frequency region, indicating at a first glance a better capacitive behavior and smaller diffusion resistance. At 900 °C, the semicircle become very small sign of a good electronic conductivity. From the intercept of the semicircle with the real axis, the equivalent series resistance (ESR) of the electrodes can be determined which gives information about the total resistance of the system comprising the electrode, the electrolyte, and separator. This resistance is ~13 and ~4 Ohm for 750 and 900 °C carbons, therefore, significantly much smaller than for the 600 °C sample (several thousand Ohms) proving the improvement of the electronic conductivity. To further improve the electrochemical performances, the 750 °C sample was mixed with carbon black. The CV exhibits a more rectangular CV curve indicating electric double layer capacitive behavior. The Nyquist plot show a smaller semi-circle when carbon black is used, the resistance being diminished to 6 Ohm. Therefore, the improvement in the conductivity allows to achieve a capacitance of 95 F/g for 750 °C/CB sample. A general trend of the capacitance evolution with the ESR is seen in Figure 10d, i.e., an increase in the capacitance with the increase of the ESR for the materials treated at 600 °C and 750 °C, therefore, for materials presenting similar specific surface areas. For the 900 °C carbon, even if the ESR is lower, the delivered capacitance is much lower than the other materials and this can be related to its lower specific surface area (Table 1).

In order to compare the performances of such materials with those reported in the literature, several electrochemical performances in H₂SO₄ were gathered in Table 3 along with their specific surface area and nitrogen content. The selected samples were limited to material exhibiting characteristics (porosity and nitrogen content) comparable with those obtained in the present work. It can be seen that all these materials present higher capacitance than our materials even if the surface area are comparable. However, it can be noticed that no strict correlation between the BET surface area and the capacitance is observed (Figure 10b). If the capacitance is plotted versus the nitrogen content, a nice increase trend of the capacitance with the increase of the nitrogen amount is seen (Figure 10e) for most reported materials in the literature, suggesting an important contribution of pseudo-capacitive reactions to the overall performance. However, it can be noticed that for our materials the capacity is lower compared to other materials and in particularly for the richer N-doped sample. In this particular case, the high resistance of these materials induced by the high amounts of oxygen (Figure 10d,f) may explain the very low capacitance. Another parameter that can be considered to explain the lower capacitance values maybe the carbon pore size. It is well known that the capacity is improved when the carbon pore size approaches the size of electrolyte ions and the maximum capacitance was demonstrated to be achieved for pore with size ~0.7 nm [16,17,42]. However, in many works this useful information regarding the micropore size is often not provided (Table 3) which makes it difficult to understand the storage mechanisms in complex doped carbons. In the present materials the micropore size is centered on ~0.6 nm, which may be considered rather small to ensure effective diffusion of electrolyte into the microporosity and the formation of the electrochemical double layer [42].

Taking into consideration these results, it can be highlighted that several carbon characteristics (conductivity, porosity and functionalities) are impacting the electrochemical capacitance. The optimal carbon must combine firstly good electronic properties and high amounts of nitrogen but also optimal porosity. Therefore, the prepared materials are meet most of these requirements; nevertheless, their performances may be improved by enlarging the micropore size and amount. An activation step already demonstrated the utility in order to improve the porosity and to achieve higher capacitance [8,43] and can be implemented further for these materials.

Table 3. Literature review on N-doped mesoporous carbon electrochemical performances in H₂SO₄ electrolyte along with their specific surface area and nitrogen content.

Material Name	SSA m ² ·g ⁻¹	Pore Volume cm ³ ·g ⁻¹	Pore Size nm	N wt %	Capacitance F·g ⁻¹	Current Rate A·g ⁻¹	Refs.
CESM-300	221	0.13	<3 nm	8.5	214	2	[44]
CA800	514	0.089	-	10.9	235	2	[45]
N-OMC	320	0.21	3.2	11.6	216	0.1	[46]
MR800	332	0.20	1.6–3.0	4.0	117	1	[47]
H-NMC-2.5	537	0.47	14.8	13.1	244	0.5	[21]
ACM-5	551	0.32	-	3.1	75.6	10 *	[48]
NNCM-0.5	593	1.7	-	5.1	170	0.1	[49]

* –mV·s⁻¹.

4. Conclusions

An eco-friendly and facile direct synthesis route based on co-assembly of a green phenolic resin (phloroglucinol/glyoxylic acid), guanine and a soft-template, to design N-doped mesoporous, is demonstrated in this work. Distinct carbon textures and high nitrogen contents could be obtained by tuning several experimental parameters. The synthesis procedure and the amount of template strongly influenced the mesoporosity but also the microporosity of the carbon while the thermal annealing induces also modification in the surface functionalities. The ¹³C NMR studies evidenced cross-linking reactions between phloroglucinol and glyoxylic acid and no covalent bonds formation with guanine. The successful assembly of the guanine with the phenolic resin via H-bondings and with the hydrophilic moieties of the template micelles resulted in ordered mesostructures with uniformly dispersed nitrogen in the carbon framework. The electrochemical performances as electrodes in supercapacitor were strongly impacted by the resistance of the materials. For low annealing temperature (600 °C) the nitrogen and oxygen content in the materials is very high inducing high resistance and consequently low capacitance. Increasing the annealing temperature led to the removal of oxygen/nitrogen groups, a decrease in the resistance and improvement of the capacitance. The maximum achieved capacitance was 97 F·g⁻¹ for materials treated at 750 °C which combines high surface area, high conductivity and proper amounts of heteroatoms.

Acknowledgments: The Réseau sur le Stockage Electrochimique de l’Energie (RS2E) is acknowledged for financial support of this project through the ANR project Storex (ANR-10-LABX-76-01). The authors thank, Loïc Vidal and Jean-Marc Le Meins for their assistance with the TEM and SAXS analysis through the IS2M technical platforms. Luc Delmotte is acknowledged for performing the NMR analysis. Barbara Daffos and Wan-Yu Tsai from CIRIMAT are acknowledged for the help provided with the electrochemical measurements.

Author Contributions: Georges Moussa performed the synthesis of the materials and their electrochemical characterization, Samar Hajar-Garreau analyzed the materials by XPS technique, Pierre-Louis Taberna and Patrice Simon supervised the electrochemistry part while Camélia Matei Ghimbeu supervised the whole work and write the manuscript. All authors reviewed the manuscript prior to the submission.

Conflicts of Interest: The authors declare no conflict of interest.

References

1. Chang, H.; Joo, S.; Chanh, P. Synthesis and characterization of mesoporous carbon for fuel cell applications. *J. Mater. Chem.* **2007**, *17*, 3078–3088. [[CrossRef](#)]
2. Eftekhari, A.; Fan, Z. Ordered mesoporous carbon and its applications for electrochemical energy storage and conversion. *Mater. Chem. Front.* **2017**, *1*, 1001–1027. [[CrossRef](#)]
3. Liang, C.; Li, Z.; Dai, S. Mesoporous carbon materials: Synthesis and modification. *Angew. Chem. Int. Ed.* **2008**, *47*, 3696–3717. [[CrossRef](#)] [[PubMed](#)]
4. Libbrecht, W.; Verberckmoes, A.; Thybaut, J.; Van der Voort, P. Soft templated mesoporous carbons: Tuning the porosity for the adsorption of large organic pollutants. *Carbon* **2017**, *116*, 528–546. [[CrossRef](#)]
5. Ma, T.-Y.; Liu, L.; Yuan, Z.-Y. Direct synthesis of ordered mesoporous carbons. *Chem. Soc. Rev.* **2013**, *42*, 3977–4003. [[CrossRef](#)] [[PubMed](#)]
6. Ndamani, J.C.; Guo, L.P. Ordered mesoporous carbon for electrochemical sensing: A review. *Anal. Chim. Acta* **2012**, *747*, 19–28. [[CrossRef](#)] [[PubMed](#)]
7. Xin, W.; Song, Y. Mesoporous carbons: Recent advances in synthesis and typical applications. *RSC Adv.* **2015**, *5*, 83239–83285. [[CrossRef](#)]
8. Deng, Y.; Xie, Y.; Zou, K.; Ji, X. Review on recent advances in nitrogen-doped carbons: Preparations and applications in supercapacitors. *J. Mater. Chem. A* **2016**, *4*, 1144–1173. [[CrossRef](#)]
9. Beguin, F.; Frackowiak, F. *Carbons for Electrochemical Energy Storage and Conversion Systems*; CRC Press: New York, NY, USA, 2010.
10. Liu, C.; Li, F.; Ma, L.; Cheng, H. Advanced Materials for Energy Storage. *Adv. Mater.* **2010**, *22*, 28–62. [[CrossRef](#)] [[PubMed](#)]
11. Simon, P.; Gogotsi, Y. Materials for electrochemical capacitors. *Nat. Mater.* **2008**, *7*, 845–854. [[CrossRef](#)] [[PubMed](#)]
12. Candelaria, S.; Shao, Y.; Zhou, W.; Li, X.; Xiao, J.; Zhang, J.; Wang, Y.; Liu, J.; Li, J.; Cao, G. Nanostructured carbon for energy storage and conversion. *Nano Energy* **2012**, *1*, 195–220. [[CrossRef](#)]
13. Conway, B. *Electrochemical Supercapacitors: Scientific Fundamentals and Technological Applications*; Kluwer Academic Plenum Publisher: New York, NY, USA, 1999.
14. Kim, K.; Park, S. Synthesis and high electrochemical capacitance of N-doped microporous carbon/carbon nanotubes for supercapacitor. *J. Electroanal. Chem.* **2012**, *673*, 58–64. [[CrossRef](#)]
15. Zhang, Q.; Uchaker, E.; Candelaria, S.; Cao, G. Nanomaterials for energy conversion and storage. *Chem. Soc. Rev.* **2013**, *42*, 3127–3171. [[CrossRef](#)] [[PubMed](#)]
16. Largeot, C.; Portet, C.; Chmiola, J.; Taberna, P.; Gogotsi, Y.; Simon, P. Relation between the Ion Size and Pore Size for an Electric Double-Layer Capacitor. *J. Am. Chem. Soc.* **2008**, *130*, 2730–2731. [[CrossRef](#)] [[PubMed](#)]
17. Raymundo-Pinero, E.; Kierzek, K.; Machnikowski, J.; Beguin, F. Relationship between the nanoporous texture of activated carbons and their capacitance properties in different electrolytes. *Carbon* **2006**, *44*, 2498–2507. [[CrossRef](#)]
18. Raymundo-Pinero, E.; Cadek, M.; Beguin, F. Tuning Carbon Materials for Supercapacitors by Direct Pyrolysis of Seaweeds. *Adv. Funct. Mater.* **2009**, *19*, 1032–1039. [[CrossRef](#)]
19. Moussa, G.; Matei Ghimbeu, C.; Taberna, P.-L.; Simon, P.; Vix-Guterl, C. Relationship between the carbon nano-onions (CNOs) surface chemistry/defects and their capacitance in aqueous and organic electrolytes. *Carbon* **2016**, *105*, 268–277. [[CrossRef](#)]
20. Garcia, B.; Candelaria, S.; Cao, G. Nitrogenated porous carbon electrodes for supercapacitors. *J. Mater. Sci.* **2012**, *47*, 5996–6004. [[CrossRef](#)]
21. Wei, J.; Zhou, D.; Sun, Z.; Deng, Y.; Xia, Y.; Zhao, D. A controllable synthesis of rich Nitrogen-Doped Ordered Mesoporous Carbon for CO₂ Capture and supercapacitors. *Adv. Funct. Mater.* **2013**, *23*, 2322–2328. [[CrossRef](#)]
22. Wang, J.; Liu, H.; Gu, X.; Wang, H.; Su, D. Synthesis of nitrogen-containing ordered mesoporous carbon as a metal-free catalyst for selective oxidation of ethylbenzene. *Chem. Commun.* **2014**, *50*, 9182–9184. [[CrossRef](#)] [[PubMed](#)]
23. Shen, G.; Sun, X.; Zhang, H.; Liu, Y.; Zhang, J.; Meka, A.; Zhou, L.; Yu, C. Nitrogen-doped ordered mesoporous carbon single crystals: Aqueous organic-organic self assembly and superior supercapacitor performance. *J. Mater. Chem. A* **2015**, *3*, 24041–24048. [[CrossRef](#)]

24. Yu, J.; Guo, M.; Muhammad, F.; Wang, A.; Zhang, F.; Qin, L.; Zhu, G. One-pot synthesis of highly ordered nitrogen-containing mesoporous carbon with resorcinol-urea-formaldehyde resin for CO₂ capture. *Carbon* **2014**, *69*, 502–514. [[CrossRef](#)]
25. Hao, G.; Liu, W.; Qian, D.; Wang, G.; Zhang, T. Structurally designed synthesis of mechanically stable poly(benzoxazine-co-resol)-based porous carbon monoliths and their application as high-performance CO₂ capture sorbents. *J. Am. Chem. Soc.* **2011**, *133*, 11378–11388. [[CrossRef](#)] [[PubMed](#)]
26. Hao, G.; Li, W.; Wang, S.; Wang, G.; Qi, L.; Lu, A. Lysine-assisted rapid synthesis of crack-free hierarchical carbon monoliths with a hexagonal array of mesopores. *Carbon* **2011**, *49*, 3762–3772. [[CrossRef](#)]
27. Zhang, W.; Zhang, Y.; Liu, J. Preparation of nitrogen hybrid ordered mesoporous carbons from melamine-phenol-formaldehyde resoles by soft-template method. *Adv. Mater. Res.* **2013**, *652*, 223–227. [[CrossRef](#)]
28. Zhong, H.; Zhang, H.; Liu, S.; Deng, C.; Wang, M. Nitrogen-enriched carbon from melamine resins with superior oxygen reduction reaction activity. *ChemSusChem* **2013**, *6*, 807–812. [[CrossRef](#)] [[PubMed](#)]
29. Xin, G.; Wang, Y.; Jia, S.; Tian, P.; Zhou, S.; Zhang, J. Synthesis of nitrogen-doped mesoporous carbon from polyaniline with an F127 template for high-performance supercapacitors. *Appl. Surf. Sci.* **2017**, *422*, 654–660. [[CrossRef](#)]
30. Matei Ghimbeu, C.; Vidal, L.; Delmotte, L.; Le Meins, J.-M.; Vix-Guterl, C. Catalyst-free soft-template synthesis of ordered mesoporous carbon tailored by phloroglucinol/glyoxylic acid environmentally friendly precursors. *Green Chem.* **2014**, *16*, 3079–3088. [[CrossRef](#)]
31. Matei Ghimbeu, C.; Soprony, M.; Sima, F.; Vaultot, C.; Vidal, L.; Le Meins, J.M.; Delmotte, L. Light-assisted evaporation induced self-assembly: An efficient approach toward ordered carbon materials. *RSC Adv.* **2015**, *5*, 2861–2868. [[CrossRef](#)]
32. Sopronyi, M.; Sima, F.; Vaultot, C.; Delmotte, L.; Bahouka, A.; Matei Ghimbeu, C. Direct synthesis of graphitic mesoporous carbon from green phenolic resins exposed to subsequent UV and IR laser irradiations. *Sci. Rep.* **2016**, *6*, 39617. [[CrossRef](#)] [[PubMed](#)]
33. Maetz, A.; Delmotte, L.; Moussa, G.; Dentzer, J.; Knopf, S.; Matei-Ghimbeu, C. Facile and sustainable synthesis of nitrogen-doped polymer and carbon porous spheres. *Green Chem.* **2017**, *19*, 2266–2274. [[CrossRef](#)]
34. Matei Ghimbeu, C.; Luchnikov, V. Hierarchical porous nitrogen-doped carbon beads derived from biosourced chitosan polymer. *Microporous Mesoporous Mater.* **2018**, *263*, 42–52. [[CrossRef](#)]
35. Jagiello, J.; Olivier, J. Carbon slit pore model incorporating surface energetical heterogeneity and geometrical corrugation. *Adsorption* **2013**, *19*, 777–783. [[CrossRef](#)]
36. Jagiello, J.; Olivier, J. 2D-NLDFT adsorption models for carbon slit-shaped pores with surface energetical heterogeneity and geometrical corrugation. *Carbon* **2013**, *55*, 70–80. [[CrossRef](#)]
37. Gogotsi, Y.; Simon, P. True Performance Metrics in Electrochemical Energy Storage. *Science* **2011**, *334*, 917–918. [[CrossRef](#)] [[PubMed](#)]
38. Nita, C.; Bensafia, M.; Vaultot, C.; Delmotte, L.; Matei Ghimbeu, C. Insights on the synthesis mechanism of green phenolic resin derived porous carbons via a salt-soft templating approach. *Carbon* **2016**, *109*, 227–238. [[CrossRef](#)]
39. Sheng, Z.-H.; Shao, L.; Chen, J.-J.; Bao, W.-J.; Wang, F.-B.; Xia, X.-H. Catalyst-free synthesis of nitrogen-doped graphene via thermal annealing graphite oxide with melamine and its excellent electrocatalysis. *ACS Nano* **2011**, *5*, 4350–4358. [[CrossRef](#)] [[PubMed](#)]
40. Wang, H.; Maiyalagan, T.; Wang, X. Review on recent progress in nitrogen-doped graphene: Synthesis, characterization, and its potential applications. *ACS Catal.* **2012**, *2*, 781–794. [[CrossRef](#)]
41. Lahaye, J.; Nanse, G.; Fioux, P.; Bagreev, A.; Broshnik, A.; Strelko, V. Chemical transformation during the carbonisation in air and the pyrolysis under argon of a vinylpyridine-divinylbenzene copolymer by X-ray photoelectron spectroscopy. *Appl. Surf. Sci.* **1999**, *147*, 153–174. [[CrossRef](#)]
42. Decaux, C.; Matei-Ghimbeu, C.; Dahbi, M.; Anouti, M.; Lemordant, D.; Beguin, F.; Vix-Guterl, C.; Raymundo-Piñero, E. Influence of electrolyte ion-solvent interactions on the performances of supercapacitors porous carbon electrodes. *J. Power Sources* **2014**, *263*, 130–140. [[CrossRef](#)]
43. Li, Z.; Guo, K.; Chen, X. Controllable synthesis of nitrogen-doped mesoporous carbons for supercapacitor applications. *RSC Adv.* **2017**, *7*, 30521–30532. [[CrossRef](#)]

44. Li, Z.; Zhang, L.; Amirkhiz, B.; Tan, X.; Xu, Z.; Wang, H.; Olsen, B.; Holt, C.; Mitlin, D. Carbonized chicken eggshell membranes with 3D Architectures as high-performance electrode materials for supercapacitors. *Adv. Energy Mater.* **2012**, *2*, 431–437. [[CrossRef](#)]
45. Li, L.; Liu, E.; Li, J.; Yang, Y.; Shen, H.; Huang, Z.; Xiang, X.; Li, W. A doped activated carbon prepared from polyaniline for high performance supercapacitors. *J. Power Sources* **2010**, *191*, 1516–1521. [[CrossRef](#)]
46. Chen, H.; Zhou, M.; Wang, Z.; Zhao, S.; Guan, S. Rich nitrogen-doped ordered mesoporous phenolic resin-based carbon for supercapacitors. *Electrochim. Acta* **2014**, *148*, 187–194. [[CrossRef](#)]
47. Fiset, E.; Rufford, T.; Seredych, M.; Bandoz, T.; Hulicova-Jurcakova, D. Comparison of melamine resin and melamine network as precursors for carbon electrodes. *Carbon* **2015**, *81*, 239–250. [[CrossRef](#)]
48. Wang, Y.; Fugetsu, B.; Wang, Z.; Gong, W.; Sakatan, I.; Morimoto, S.; Hoshimoto, Y.; Endo, M.; Dresselhaus, M.; Terrones, M. Nitrogen-doped porous carbon monoliths from polyacrylonitrile (PAN) and carbon nanotubes as electrodes for supercapacitors. *Sci. Rep.* **2017**, *7*, 40259. [[CrossRef](#)] [[PubMed](#)]
49. Yang, X.; Ma, H.; Zhang, G. Nitrogen-doped mesoporous carbons for supercapacitor electrodes with high specific volumetric capacitance. *Langmuir* **2017**, *33*, 3975–3981. [[CrossRef](#)] [[PubMed](#)]



© 2018 by the authors. Licensee MDPI, Basel, Switzerland. This article is an open access article distributed under the terms and conditions of the Creative Commons Attribution (CC BY) license (<http://creativecommons.org/licenses/by/4.0/>).